# Predissociation Measurements of Bond Dissociation Energies



| | |
|---|---|
| Journal: | *Accounts of Chemical Research* |
| Manuscript ID | ar-2018-00526g.R1 |
| Manuscript Type: | Article |
| Date Submitted by the Author: | 07-Dec-2018 |
| Complete List of Authors: | Morse, Michael; University of Utah, Department of Chemistry |
| | |

# Predissociation Measurements of Bond Dissociation Energies

Michael D. Morse*

Department of Chemistry

University of Utah,

315 South 1400 East,

Salt Lake City, Utah 84112, United States

**CONSPECTUS:** A fundamental need in chemistry is understanding the chemical bond, for which the most quantitative measure is the bond dissociation energy (BDE). While BDEs of chemical bonds formed from the lighter main group elements are generally well-known and readily calculated by modern computational chemistry, chemical bonds involving the transition metals, lanthanides, and actinides remain computationally extremely challenging. This is due to the simultaneous importance of electron correlation, spin-orbit interaction, and other relativistic effects, coupled with the large numbers of low-lying states that are accessible in systems with open *d*- or *f*-subshells. The development of efficient and accurate computational methods for these species is currently a major focus of the field.

An obstacle to this effort has been the scarcity of highly precise benchmarks for the BDEs of M-X bonds. For most of the transition metal, lanthanide, or actinide systems, tabulated BDEs of M-X bonds have been determined by Knudsen effusion mass spectrometric measurements of high-temperature equilibria. The measured ion signals are converted to pressures and activities of the species involved in the equilibrium, and the equilibrium constants are then analyzed using a van't Hoff plot or the third-law method to extract the reaction enthalpy, which is extrapolated to 0K to obtain the BDE. This procedure introduces errors at every step, and ultimately leads to BDEs that are typically uncertain by 2-20 kcal $mol^{-1}$ (0.1-1 eV). A second method in common use employs a thermochemical cycle in which the ionization energies of the MX molecule and M atom are combined with the BDE of the $M^+$-X bond, obtained via guided ion beam mass spectrometry, to yield the BDE of the neutral, M-X. When accurate values of all three components of the cycle are available, this method yields good results – but only rarely are all three values available.

We have recently implemented a new method for the precise measurement of BDEs in molecules with large densities of electronic states that is based on the rapid predissociation of these species as soon as the ground separated atom limit is exceeded. When a sharp predissociation threshold is observed, its value directly provides the BDE of the system.

With this method, we are able in favorable cases to determine M-X BDEs to an accuracy of ~0.1 kcal $mol^{-1}$ (0.004 eV). The method is generally applicable to species that have a high density of states at the ground separated atom limit, and has been used to measure the BDEs of more than 50 transition metal – main group MX molecules thus far. In addition, a number of metal-metal BDEs have also been measured with this method. There are good prospects for the extension of the method to polyatomic systems and to lanthanide and actinide-containing molecules. These precise BDE measurements provide chemical trends for the BDEs across the transition metal series, as well as crucial benchmarks for the development of efficient and accurate computational methods for the *d*- and *f*-block elements.

## 1. INTRODUCTION

The chemical bond is among the most fundamental concepts in all of chemistry, and the bond dissociation energy (BDE) provides the most quantitatively useful description of the bond. BDEs are particularly valuable for thermochemical calculations, which allow reaction energies to be calculated as the sum of the BDEs of bonds that are broken minus the BDEs of the bonds that are formed. As with all thermochemical quantities, BDEs are related to other thermochemical quantities through thermochemical cycles. These include cycles relating to enthalpies of formation:

$$\Delta H_{f,0K}(AB) = \Delta H_{f,0K}(A) + \Delta H_{f,0K}(B) - D_0(AB), \quad (1.1)$$

and those relating BDEs of different charge states, such as neutrals and cations:

$$D_0(AB) + IE(A) = IE(AB) + D_0(A^+\text{-}B) \quad (1.2)$$

and neutrals and anions:

$$EA(AB) + D_0(AB) = D_0(A^-\text{-}B) + EA(A). \quad (1.3)$$

In these equations, $\Delta H_{f,0K}(X)$ is the 0K formation enthalpy of X, $D_0(AB)$ is the 0K bond dissociation energy of AB, IE(X) and EA(X) are the ionization energy and electron affinity of X, and $D_0(A^{\pm} - B)$ is the 0K dissociation energy of the $AB^{\pm}$ ion into $A^{\pm}$ and B. In the examples of Equations (1.2) and (1.3), if three of the four quantities are independently known, the cycle may be solved to determine the fourth quantity. If all four are known, a lack of self-consistency allows problematic cases to be identified; alternatively, if self-consistency is present, the proposed error limits may be verified.

In addition to their thermochemical value, bond dissociation energies provide a stringent test of quantum chemical computational methods. While BDEs are notoriously difficult to compute to high accuracy, in part because they require electron correlation to be treated to the same level of accuracy in the united molecule as in the separated fragments, it is precisely because of this difficulty that accurate BDE measurements provide useful and important benchmarks for computational chemistry. Validation of computational methods

using accurate benchmarks is absolutely crucial if theory is to be used for the accurate prediction of reaction thermochemistry.

A current focus in computational chemistry is improving the accuracy of calculations on transition metal, lanthanide, and actinide molecules. Although current computational methods often provide results of high accuracy (within 1 kcal $mol^{-1}$ or 0.04 eV, termed "chemical accuracy")[1] for light main-group elements, the *d*- and *f*-block metals present much greater difficulties.[1-7] For those species with open *d*- or *f*-subshells, the high density of states complicates computations severely, requiring a particularly high level of attention to the electron correlation problem. In addition, heavy metal systems exhibit large relativistic effects, including spin-orbit interactions. All of these phenomena must be treated properly in order to compute accurate thermochemistry. In addition to the computational difficulties, a major problem lies with the available experimental data. For neutral diatomic metals and metal-ligand diatomics, most of the available BDEs derive from high-temperature Knudsen effusion measurements of gas phase equilibria and are subject to errors much greater than the desired 1 kcal $mol^{-1}$.[8] Typically, these errors lie in the range of 2-20 kcal $mol^{-1}$ (0.1-1 eV), a far cry from the desired chemical accuracy. For cations, many of the BDEs are available from the results of guided ion beam mass spectrometry (GIBMS),[9-15] with error limits typically in the range of 0.03 – 0.4 eV. The best of these results meet the standard of "chemical accuracy," but many do not. In a few cases,[16-20] molecular ionization energies are accurately known from pulsed field ionization-zero electron kinetic energy (PFI-ZEKE) studies. For these molecules, accurate BDEs for cations can be converted into accurate BDEs for the corresponding neutrals via Equation (1.2). For many species of interest, however, no BDE measurements exist at all. In this Account, we present a new, general method for the precise measurement of BDEs in molecules with high densities of electronic states.

## 2. PREDISSOCIATION

The phenomenon of predissociation is illustrated in Figure 1 for the hydroxyl radical, a molecule with a relatively low density of electronic states.[21, 22] The lower rovibronic levels of the $A^2\Sigma^+$ state decay by fluorescence to the ground $X^2\Pi$ state, but higher levels couple via spin-orbit interaction to the repulsive $^4\Sigma^-$ and $^4\Pi$ states, causing these levels to dissociate to ground state O and H atoms.[23] The result is that rovibronic levels of the $A^2\Sigma^+$ state, which correlates to the O $^1$D + H $^2$S separated atom limit, fall apart long before this limit is reached. The phenomenon of molecular dissociation occurring before the corresponding separated atom limit is reached is called *predissociation*. It is the key phenomenon that allows bond dissociation energies of transition metal molecules to be measured to high precision.

For OH in its $A^2\Sigma^+$ state, rotational levels above 40,031 cm$^{-1}$ in the v=2 vibrational level undergo predissociation.[23] This places an upper limit on the BDE of 40,031 cm$^{-1}$ (4.963 eV), greatly exceeding the accepted BDE of 4.4113(3) eV.[24] The predissociation threshold observed in OH provides a poor estimate of the bond energy, due to the low density of electronic states in this species.

To place the density of states in OH in perspective, the ground separated atom limit for OH is O $^3$P + H $^2$S, comprising 18 electronic states; the next separated atom limit, O $^1$D + H $^2$S, lies 15,868 cm-1 higher in energy, generating 10 additional states. Thus, within 2 eV (50 kcal mol$^{-1}$), only 28 states arise for the OH molecular system. This low density of states leads to well-separated, readily interpreted spectroscopic features. Most diatomic molecules containing an open *d*-subshell transition metal atom exhibit a far greater density of states, leading to a near-continuum of spectroscopic features at energies close to the ground separated atom limit. The high density of electronic states in these cases allows predissociation to set in as soon as the ground separated atom limit is exceeded in energy, enabling high-precision measurements of BDEs by the observation of a sharp predissociation threshold.

As an example, Figure 2 displays 15 of the low-lying Λ-S potential energy curves for YC, along with 4 low-lying Λ-S curves for the cation, $YC^+$. However, these represent only a small fraction of the states arising from the four lowest separated atom limits of Y + C. In addition to the 15 Λ-S states shown, an additional 63 Λ-S states arising from these separated atom limits have either been omitted or simply not calculated. It would be impossible to display all of these curves in the same figure. With so many electronic states present, it is easy to imagine that a YC molecule that is excited above the ground separated atom limit will find a way to hop from curve to curve and quickly dissociate.

To quantify the density of electronic states further, consider the number of electronic states expected near the separated atom limit in the transition metal molecules, YC, TaSi, TiSe, WC, AlNi, VS, TiCo, and $V_2$. It is straightforward to calculate the total number of states available to the separated atoms below a given separated atom energy using the known atomic energy levels.[25] The results are listed in Table 1, and displayed in Figure 3 as a function of energy ($cm^{-1}$), along with the results for OH. The number of states available in the transition metal molecules is huge, particularly if one considers states that arise from separated atom limits lying within 5000 $cm^{-1}$ of the ground limit. At this energy, the number of states in the listed transition metal molecules exceeds that of OH by a factor ranging from 5 to nearly 200. Further, many of these molecular potential energy curves dip below the ground separated atom limit, leading to a nearly continuous absorption spectrum as one approaches the bond dissociation energy. Avoided curve crossings, spin-orbit interaction, and nonadiabatic coupling effects then allow molecules excited above the dissociation limit to fall apart almost as soon as the limit is exceeded. At a minimum, the observation of a sharp predissociation threshold provides an upper limit to the BDE of the molecule.

## 3. RESONANT TWO-PHOTON IONIZATION SPECTROSCOPY

We employ laser ablation of a metal sample, followed by supersonic expansion in helium, perhaps seeded with a small percentage of a reactant gas, to prepare molecular beams containing transition metal molecules that have been cooled to temperatures in the range of 5-20K. The method is general, can be used with any metallic element or alloy, and when combined with reactant gases such as $CH_4$, $NH_3$, $N_2O$, $SiH_4$, $H_2S$, or $H_2Se$ can be used to prepare cold gas-phase molecular samples of transition metal molecules like MC, MN, MO, MSi, MS, or MSe.

The molecular beam passes through a skimmer into a second chamber where a resonant two-photon ionization (R2PI) process is used to record mass-analyzed spectra of the constituents of the beam. A tunable laser is scanned across a region where the molecule of interest is expected to absorb, and after a short time delay (~20 ns), this is followed by a second laser pulse that is capable of ionizing any excited states that have been produced, but which cannot ionize the molecular ground state in a one-photon process. Ions are then detected in a time-of-flight mass spectrometer. The two-photon ionization process is illustrated in Figure 4.

When the molecule exhibits a high density of states near the dissociation threshold, perturbations among the states allow dark states to pick up spectral intensity. This leads to an extremely dense absorption spectrum that often appears to be continuous. However, when the dissociation limit is exceeded and rapid predissociation sets in, the excited states fall apart more rapidly than they can be ionized. The result is a sharp drop in signal that allows the BDE to be determined to high precision, as is illustrated Figure 5 for diatomic TiCo, produced by laser ablation of a 1:1 Ti:Co alloy.[26]

The question remains: Does the observed predissociation threshold correspond to a true thermochemical BDE, or is it merely an upper limit on this quantity? For one example, $V_2$, we have solid evidence that the measured predissociation threshold provides an

exceptionally good measurement of the true thermochemical BDE. For $V_2$ and $V_2^+$, we have measured the BDEs as $D_0(V_2) = 22{,}201(1)$ cm$^{-1}$ and $D_0(V^+\text{-}V) = 25{,}326(15)$ cm$^{-1}$ by observing the onset of predissociation in a quasi-continuous R2PI or photodissociation action spectrum, respectively.[26, 27] The ionization energies have been independently measured as $IE(V) = 54{,}411.67(17)$ cm$^{-1}$ and $IE(V_2) = 51{,}271.14(50)$ cm$^{-1}$ using pulsed field ionization-zero electron kinetic energy spectroscopy (PFI-ZEKE).[28, 29] These quantities are tied through equation (1.2), which may be rearranged as

$$D_0(AB) + IE(A) - IE(AB) - D_0(A^+\text{-}B) = 0. \quad (3.1)$$

The thermochemical cycle is illustrated in Figure 6. Combining the quantities on the right side of Equation (3.1) and propagating the error, a value of $15.50 \pm 15$ cm$^{-1}$ is obtained, clearly demonstrating that when a sufficient density of states is available, the observed predissociation threshold provides an extremely accurate measure of the BDE of the molecule. Table 2 provides a list of metal cluster BDEs measured in the Morse group using this method.

Predissociation thresholds have also been employed in a few other research groups to measure BDEs of transition metal molecules, particularly for VNb,[28] $Mo_2$,[30] $Ni_2^+$,[31] $Zr_2^+$,[32] $Nb_2^+$,[32] and $Nb_3^+$-Nb.[32] Some of the earliest work along these lines was performed in Ben Freiser's group on ions trapped in an ion cyclotron resonance cell, irradiated with the output of a conventional cw light source that was wavelength selected to a 1 nm range using a monochromator. Due to the wide band pass of the monochromator and the low intensity of this light source, rather broad error limits (0.13 eV or greater) were reported. Nevertheless, these results clearly demonstrated the value of predissociation measurements of BDEs in gas-phase transition metal ions. Results obtained by these groups are provided in Table 3.

## 4. BOND ENERGIES OF TRANSITION METAL – MAIN GROUP MOLECULES

Although the main group elements lead to a lower density of states when combined with a transition metal atom, our success in measuring BDEs for species such as AlV, AlCo, and AlNi suggested that we might be able to apply these same methods to transition metal-main group molecules. Beginning in 2015, we began these experiments and immediately found success. After an initial study of VC, VN, and VS,[33] we began studies of the group 4 and 5 transition metal selenides and silicides, MSe and MSi.[34, 35] The experiments provided very clear-cut predissociation thresholds and precise values of the corresponding BDEs. Figures 7-9 display the R2PI spectra that provide the BDEs of VS, TaSi, and TiSe as examples of the method. In these studies we have avoided examining the predissociation behavior of molecules containing transition metal atoms with $d^5$ or $d^{10}$ configurations (Cr, Mn, Cu, Zn, Mo, Tc, Pd, Ag, Cd, Re, Au, and Hg), because the ground separated atom limits of these species generate far fewer electronic states. This makes them less likely to predissociate immediately at the ground separated atom limit. The remaining transition metal atoms have $^{(2S+1)}$D or $^{(2S+1)}$F ground terms, which result in a much greater density of states. We have now measured BDEs of more than 50 different diatomic MX molecules; these values are provided in Table 4. In addition to the results in Table 4, we have also measured the BDE of ThC, which is 5.060(3) eV.[36] This is the only *f*-block molecule we have investigated thus far.

It should be noted that the error limits quoted in Tables 2 and 4 assume that rapid predissociation sets in as soon as the ground separated atom limit is exceeded. The error limits include the effects of finite laser linewidth, calibration uncertainties, and the sharpness of the final drop to baseline in the scan over the predissociation threshold. We are unable to estimate the magnitude of any barriers to dissociation that might prevent predissociation at the thermochemical threshold, so these effects are excluded from the error estimate. In most cases, the drop to baseline is quite abrupt, and we believe no barrier to predissociation exists.

For the relatively few examples where $D_0(MX)$ is known from predissociation measurements, $D_0(M^+\text{-}X)$ is known from GIBMS studies, and IE(MX) is known from PFI-ZEKE studies, the cycle given in Equation (3.1) may be tested for consistency. The results are listed in Table 5. This comparison shows that the cycle closes within the propagated error limits in most cases; the only counterexamples are one of the three studies of $VC/VC^+$ and the study of $CoC/CoC^+$. It seems that the error limits in the one GIBMS study of $VC^+$ were underestimated; similarly, the GIBMS study of $CoC^+$ may deserve reexamination as well.

## 5. CONCLUSIONS AND FUTURE OUTLOOK

The observation of a sharp predissociation threshold in a dense, quasi-continuous spectrum of a molecule with a high density of states is proving to be a highly effective means of quickly determining BDEs for a wide variety of transition metal molecules. So far we have applied this method to measure BDEs for transition metal dimers and small clusters, a few cluster cations, and 14 MC, 2 MN, 18 MSi, 15 MS, 9 MSe, and one MCl species. The method can be extended to a wide variety of other species, including small polyatomics. In a recent unpublished study probing the BDE of YC for example, accidental production of triatomic YCH allowed $D_0(Y\text{-}CH)$ to be determined as 4.102(3) eV. Other polyatomics may be similarly studied, if the density of states is sufficient, the molecule can be produced cleanly, and the BDE falls below ~6 eV, which is the current limit of our laser system.

An important direction will be to measure the BDEs of MO molecules. These measurements will be restricted to MO molecules from the latter portion of the periodic table (groups 8, 9, and 10), because for most of the early MO molecules the ionization energy of the molecule is less than the dissociation energy. In our experiments, these molecules will undergo direct one-photon ionization before they fall apart and no sharp drop in signal will be observed. The BDEs of the late transition metal oxides can be measured by these methods, and will be of considerable interest in modeling their bulk oxide phases.

The late 4*d* and 5*d* transition metal carbides, MC, are likewise of considerable interest. Knudsen effusion studies of these species show them to be very strongly bound, possibly above the range that can currently be accessed with reasonable laser intensity in our group. For these molecules (RuC, RhC, OsC, IrC, PtC), it may be necessary to implement a resonant three-photon ionization scheme, in which one wavelength is used to populate an excited state, a second photon scans over the dissociation limit, and a third photon is used for ionization. Such a scheme introduces several possibilities for artifacts, and will need to be carefully implemented.

Other diatomics that are easily amenable to these measurements are the metal borides, MB, and the metal halides, MF, MCl, MBr, and MI. Pseudo-halides such as MCN and $MC_2H$ may also be amenable to these studies. We would like to extend the work to additional metal nitrides, phosphides, and perhaps arsenides (MN, MP, and MAs), but have some concerns because the $^4S^o$ ground terms of the pnictogens lead to fewer electronic states than the $^2P^o$ or $^3P$ ground terms of the group 13, 14, 16, or 17 atoms. Still, the apparent success of the method in obtaining BDEs of TiN and VN is promising.

Systematic studies of the BDEs of lanthanide-containing molecules will likewise be of considerable interest, as the 5d contributions to the chemical bonding are expected to vary significantly across the series. The actinides are also of considerable interest, but our work there will be limited to thorium and uranium molecules.

As another extension of this work, we would like to use predissociation techniques to measure the BDEs of cationic molecules/complexes, in part to complete the thermochemical cycle and verify the assumption that the molecule falls apart at the precise thermochemical threshold. For cases in which good measurements of the ionization energy exist, a zero thermochemical defect will allow us to verify this assumption for additional molecules beyond $V_2/V_2^+$. Cations also provide another important advantage: by mass-selecting a cation prior to photofragmentation, it is possible to more cleanly study complicated species.

A potential problem for neutral molecules is that the signal for the molecule of interest may be obscured by larger clusters fragmenting into the mass of interest, leading to a false signal at that mass. If the molecule is mass-selected prior to photolysis, as is possible for cation-based work, this issue can be circumvented. Thus, we anticipate being able to measure cation BDEs of larger cationic species, like $M^+$-$C_6H_6$ or $M^+$-$C_5H_5$ more readily than can be done for neutrals.

All of this work is geared toward establishing a broad, highly precise database of transition metal-ligand (or metal-metal) BDEs that will be useful for understanding the chemical bonds and for the calibration of quantum chemical methods as well.

## AUTHOR INFORMATION

**Corresponding Author**

*E-mail: morse@chem.utah.edu. Phone: (801) 581-8319. Fax: (801) 581-8433.

ORCID

Michael D. Morse: 0000-0002-2386-7315

**Notes**

The author declares no competing financial interest.

**Biographical Information**

**Michael D. Morse's** research interests are in the electronic structure, electronic spectroscopy, and chemical bonding of small metal and semiconductor-containing molecules, particularly those containing d-block or f-block elements. He received his B.S. degree from Haverford College and his Ph.D. from the University of Chicago under the supervision of Karl F. Freed and Stuart A. Rice. He performed postdoctoral research at Rice University with Richard E. Smalley and is currently a professor at the University of Utah.

## ACKNOWLEDGMENTS

This work was supported by the National Science Foundation, most recently under Grant No. CHE-1664962. Eric Johnson, Dan Matthew, Andrew Sevy, Jason Sorensen, and Dakota Merriles are thanked for their many contributions.

## REFERENCES


(1) DeYonker, N. J.; Peterson, K. A.; Steyl, G.; Wilson, A. K.; Cundari, T. R. Quantitative Computational Thermochemistry of Transition Metal Species. *J. Phys. Chem. A* **2007**, *111*, 11269-11277.

(2) DeYonker, N. J.; Williams, T. G.; Imel, A. E.; Cundari, T. R.; Wilson, A. K. Accurate Thermochemistry for Transition Metal Complexes from First-Principles Calculations. *J. Chem. Phys.* **2009**, *131*, 024106.

(3) Mayhall, N. J.; Raghavachari, K.; Redfern, P. C.; Curtiss, L. A. Investigation of Gaussian4 Theory for Transition Metal Thermochemistry. *J. Phys. Chem. A* **2009**, *113*, 5170-5175.

(4) Luo, S.; Averkiev, B.; Yang, K. R.; Xu, X.; Truhlar, D. G. Density Functional Theory of Open-Shell Systems. The 3d-Series Transition-Metal Atoms and Their Cations. *J. Chem. Theory Comput.* **2014**, *10*, 102-121.

(5) Manivasagam, S.; Laury, M. L.; Wilson, A. K. Pseudopotential-Based Correlation Consistent Composite Approach (rp-ccCA) for First- and Second-Row Transition Metal Thermochemistry. *J. Phys. Chem. A* **2015**, *119*, 6867-6874.

(6) Xu, X.; Zhang, W.; Tang, M.; Truhlar, D. G. Do Practical Standard Coupled Cluster Calculations Agree Better Than Kohn-Sham Calculations with Currently Available Functionals When Compared to the Best Available Experimental Data for Dissociation Energies of Bonds to 3d Transition Metals? *J. Chem. Theory Comput.* **2015**, *11*, 2036-2052.

(7) Sharkas, K.; Gagliardi, L.; Truhlar, D. G. Multiconfiguration Pair-Density Functional Theory and Complete Active Space Second Order Perturbation Theory. Bond Dissociation Energies of FeC, NiC, FeS, NiS, FeSe, and NiSe. *J. Phys. Chem. A* **2017**, *121*, 9392-9400.

(8) Gingerich, K. A. Mass Spectrometric Determination of Bond Energies of High-Temperature Molecules. *Chimia* **1972**, *26*, 619-623.

(9) Aristov, N.; Armentrout, P. B. Bond Energy-Bond Order Relations in Transition-Metal Bonds: Vanadium. *J. Am. Chem. Soc.* **1984**, *106*, 4065-4066.

(10) Aristov, N.; Armentrout, P. B. Reaction Mechanisms and Thermochemistry of Vanadium Ions with Ethane, Ethene and Ethyne. *J. Am. Chem. Soc.* **1986**, *108*, 1806-1819.

(11) Clemmer, D. E.; Sunderlin, L. S.; Armentrout, P. B. Ammonia Activation by $V^+$: Electronic and Translational Energy Dependence. *J. Phys. Chem.* **1990**, *94*, 208-217.

(12) Clemmer, D. E.; Elkind, J. L.; Aristov, N.; Armentrout, P. B. Reaction of $Sc^+$, $Ti^+$, and $V^+$ with CO. $MC^+$ and $MO^+$ Bond Energies. *J. Chem. Phys.* **1991**, *95*, 3387-3393.

(13) Haynes, C. L.; Chen, Y.-M.; Armentrout, P. B. The Potential Energy Surface for Activation of Methane by $Co^+$: An Experimental Study. *J. Phys. Chem.* **1995**, *99*, 9110-9117.

(14) Sievers, M. R.; Chen, Y. M.; Haynes, C. L.; Armentrout, P. B. Activation of $CH_4$, $C_2H_6$, and $C_3H_8$ by Gas-Phase $Nb^+$ and the Thermochemistry of Nb-Ligand Complexes. *Int. J. Mass Spectrom.* **2000**, *195*, 149-170.

(15) Armentrout, P. B. Threshold Collision-Induced Dissociations for the Determination of Accurate Gas-Phase Binding Energies and Reaction Barriers. *Topics in Current Chemistry* **2003**, *225*, 233-262.

(16) Huang, H.; Chang, Y. C.; Luo, Z.; Shi, X.; Lam, C.-S.; Lau, K.-C.; Ng, C. Y. Rovibronically Selected and Resolved Two-Color Laser Photoionization and Photoelectron Study of Cobalt Carbide Cation. *J. Chem. Phys.* **2013**, *138*, 094301.

(17) Huang, H.; Luo, Z.-H.; Chang, Y. C.; Lau, K.-C.; Ng, C. Y. State-to-State Photoionization Dynamics of Vanadium Nitride by Two-Color Laser Photoionization and Photoelectron Methods. *Chin. J. Chem. Phys.* **2013**, *26*, 669-678.

(18) Luo, Z.; Huang, H.; Chang, Y.-C.; Zhang, Z.; Yin, Q.-Z.; Ng, C. Y. Rotationally Resolved State-to-State Photoionization and Photoelectron Study of Titanium Carbide and Its Cation ($TiC/TiC^+$). *J. Chem. Phys.* **2014**, *141*, 144307.

(19) Luo, Z.; Huang, H.; Zhang, Z.; Chang, Y.-C.; Ng, C. Y. Rotationally Resolved State-to-State Photoelectron Study of Niobium Carbide Radical. *J. Chem. Phys.* **2014**, *141*, 024304.

(20) Chang, Y. C.; Luo, Z.; Pan, Y.; Zhang, Z.; Song, Y.-N.; Kuang, S. Y.; Yin, Q. Z.; Lau, K.-C.; Ng, C. Y. Rotationally Resolved State-to-State Photoionization and the Photoelectron Study of Vanadium Monocarbide and Its Cations (VC/VC$^+$). *Phys. Chem. Chem. Phys.* **2015**, *17*, 9780-9793.

(21) Raab, F.; Bergeman, T.; Lieberman, D.; Metcalf, H. Precision Study of the $A^2\Sigma^+$ State of the OH Radical. *Phys. Rev. A* **1981**, *24*, 3120-3135.

(22) Bergeman, T.; Erman, P.; Haratym, Z.; Larsson, M. Experimental and Theoretical Studies of OD $A^2\Sigma^+$ State Lifetimes and Predissociations. *Phys. Scr.* **1981**, *23*, 45-53.

(23) Huber, K. P.; Herzberg, G. *Constants of Diatomic Molecules*; Van Nostrand Reinhold: New York, 1979; Vol. IV.

(24) Ruscic, B.; Pinzon, R. E.; von Laszewski, G.; Kodeboyina, D.; Burcat, A.; Leahy, D.; Montoya, D.; Wagner, A. F. Active Thermochemical Tables: Thermochemistry for the 21st Century. *Journal of Physics: Conference Series* **2005**, *16*, 561-570. Accessed at https://atct.anl.gov/ on Dec. 5, 2018.

(25) Kramida, A. E.; Ralchenko, Yu.; Reader, J.; and NIST ASD Team *Atomic Spectra Database (Version 5.6.1)*; National Institute of Standards and Technology, Gaithersburg, MD, 2018.

(26) Spain, E. M.; Morse, M. D. Bond Strengths of Transition Metal Dimers: TiV, $V_2$, TiCo, and VNi. *J. Phys. Chem.* **1992**, *96*, 2479-2486.

(27) Russon, L. M.; Heidecke, S. A.; Birke, M. K.; Conceicao, J.; Morse, M. D.; Armentrout, P. B. Photodissociation Measurements of Bond Dissociation Energies: $Ti_2^+$, $V_2^+$, $Co_2^+$, and $Co_3^+$. *J. Chem. Phys.* **1994**, *100*, 4747-4755.

(28) James, A. M.; Kowalczyk, P.; Langlois, E.; Campbell, M. D.; Ogawa, A.; Simard, B. Resonant Two Photon Ionization Spectroscopy of the Molecules $V_2$, VNb, $Nb_2$. *J. Chem. Phys.* **1994**, *101*, 4485-4495.

(29) Yang, D. S.; James, A. M.; Rayner, D. M.; Hackett, P. A. Pulsed Field Ionization Zero Kinetic Energy Photoelectron Spectroscopy of the Vanadium Dimer Molecule. *J. Chem. Phys.* **1995**, *102*, 3129-3134.

(30) Simard, B.; Lebeault-Dorget, M.-A.; Marijnissen, A.; ter Meulen, J. J. Photoionization Spectroscopy of Dichromium and Dimolybdenum: Ionization Potentials and Bond Energies. *J. Chem. Phys.* **1998**, *108*, 9668-9674.

(31) Asher, R. L.; Bellert, D.; Buthelezi, T.; Brucat, P. J. The Bond Strength of $Ni_2^+$. *Chem. Phys. Lett.* **1994**, *224*, 529-532.

(32) Aydin, M.; Lombardi, J. R. Multiphoton Fragmentation Spectra of Zirconium and Niobium Cluster Cations. *Int. J. Mass Spectrom.* **2004**, *235*, 91-96.

(33) Johnson, E. L.; Davis, Q. C.; Morse, M. D. Predissociation Measurements of Bond Dissociation Energies: VC, VN, and VS. *J. Chem. Phys.* **2016**, *144*, 234306.

(34) Sorensen, J. J.; Persinger, T. D.; Sevy, A.; Franchina, J. A.; Johnson, E. L.; Morse, M. D. Bond Dissociation Energies of Diatomic Transition Metal Selenides: TiSe, ZrSe, HfSe, VSe, NbSe, and TaSe. *J. Chem. Phys.* **2016**, *145*, 214308.

(35) Sevy, A.; Sorensen, J. J.; Persinger, T. D.; Franchina, J. A.; Johnson, E. L.; Morse, M. D. Bond Dissociation Energies of Diatomic Transition Metal Silicides: TiSi, ZrSi, HfSi, VSi, NbSi, and TaSi. *J. Chem. Phys.* **2017**, *147*, 084301.

(36) Sevy, A.; Matthew, D. J.; Morse, M. D. Bond Dissociation Energies of TiC, ZrC, HfC, ThC, NbC, and TaC. *J. Chem. Phys.* **2018**, *149*, 044306.

(37) Behm, J. M.; Brugh, D. J.; Morse, M. D. Spectroscopic Analysis of the Open 3d Subshell Transition Metal Aluminides: AlC, AlCr, and AlCo. *J. Chem. Phys.* **1994**, *101*, 6487-6499.

(38) Sickafoose, S. M.; Langenberg, J. D.; Morse, M. D. Rotationally Resolved Spectra of Isovalent NbCr and VCr. *J. Phys. Chem. A* **2000**, *104*, 3521-3527.

(39) Arrington, C. A.; Blume, T.; Morse, M. D.; Doverstål, M.; Sassenberg, U. Bond Strengths of Transition Metal Diatomics: $Zr_2$, YCo, YNi, ZrCo, ZrNi, NbCo, and NbNi. *J. Phys. Chem.* **1994**, *98*, 1398-1406.

(40) Behm, J. M.; Arrington, C. A.; Morse, M. D. Spectroscopic Studies of Jet-Cooled AlNi. *J. Chem. Phys.* **1993**, *99*, 6409-6415.

(41) Matthew, D. J.; Oh, S. H.; Sevy, A.; Morse, M. D. The Bond Length and Bond Energy of Gaseous CrW. *J. Chem. Phys.* **2016**, *144*, 214306.

(42) Morse, M. D.; Hansen, G. P.; Langridge-Smith, P. R. R.; Zheng, L.-S.; Geusic, M. E.; Michalopoulos, D. L.; Smalley, R. E. Spectroscopic Studies of the Jet-Cooled Nickel Dimer. *J. Chem. Phys.* **1984**, *80*, 5400-5405.

(43) Pinegar, J. C.; Langenberg, J. D.; Arrington, C. A.; Spain, E. M.; Morse, M. D. $Ni_2$ Revisited: Reassignment of the Ground Electronic State. *J. Chem. Phys.* **1995**, *102*, 666-674.

(44) Taylor, S.; Spain, E. M.; Morse, M. D. Resonant Two-Photon Ionization Spectroscopy of Jet-Cooled NiPt. *J. Chem. Phys.* **1990**, *92*, 2698-2709.

(45) Langenberg, J. D.; Morse, M. D. Bond Energies of Transition Metal Dimers: TiZr, TiNb, and ZrV. *Chem. Phys. Lett.* **1995**, *239*, 25-30.

(46) Taylor, S.; Lemire, G. W.; Hamrick, Y. M.; Fu, Z.; Morse, M. D. Resonant Two-Photon Ionization Spectroscopy of Jet-Cooled $Pt_2$. *J. Chem. Phys.* **1988**, *89*, 5517-5523.

(47) Fu, Z.; Russon, L. M.; Morse, M. D.; Armentrout, P. B. Photodissociation Measurements of Bond Dissociation Energies: $D_0(Al_2\text{-}Al)$, $D_0(TiO^+\text{-}Mn)$, and $D_0(V_2^+\text{-}V)$. *Int. J. Mass Spectrom.* **2001**, *204*, 143-157.

(48) Hettich, R. L.; Freiser, B. S. Spectroscopic and Thermodynamic Investigations of Transition-Metal Cluster Ions in the Gas Phase: Photodissociation of $MFe^+$. *J. Am. Chem. Soc.* **1987**, *109*, 3537-3542.

(49) Hettich, R. L.; Jackson, T. C.; Stanko, E. M.; Freiser, B. S. Gas-Phase Photodissociation of Organometallic Ions. Bond Energy and Structure Determinations. *J. Am. Chem. Soc.* **1986**, *108*, 5086-5093.

(50) Hettich, R. L.; Freiser, B. S. Gas-Phase Photodissociation of $FeCH_2^+$ and $CoCH_2^+$: Determination of the Carbide, Carbyne, and Carbene Bond Energies. *J. Am. Chem. Soc.* **1986**, *108*, 2537-2540.

(51) Hettich, R. L.; Freiser, B. S. Heteronuclear Transition-Metal Cluster Ions in the Gas Phase. Photodissociation and Reactivity of Vanadium-Iron Cluster Ion ($VFe^+$). *J. Am. Chem. Soc.* **1985**, *107*, 6222-6226.

(52) Cassady, C. J.; Freiser, B. S. Determination of the $Fe^+$-OH and $Co^+$-H Bond Energies by Deprotonation Reactions and by Photodissociation. *J. Am. Chem. Soc.* **1984**, *106*, 6176-6179.

(53) Matthew, D. J.; Tieu, E.; Morse, M. D. Determination of the Bond Dissociation Energies of FeX and NiX (X = C, S, Se). *J. Chem. Phys.* **2017**, *146*, 144310.

(54) Sevy, A.; Tieu, E.; Morse, M. D. Bond Dissociation Energies of FeSi, RuSi, OsSi, CoSi, RhSi, IrSi, NiSi, and PtSi. *J. Chem. Phys.* **2018**, *149*, 174307.

(55) Sevy, A.; Huffaker, R. F.; Morse, M. D. Bond Dissociation Energies of Tungsten Molecules: WC, WSi, WS, WSe, and WCl. *J. Phys. Chem. A* **2017**, *121*, 9446-9457.

(56) Suo, B.; Balasubramanian, K. Spectroscopic Constants and Potential Energy Curves of Yttrium Carbide (YC). *The Journal of Chemical Physics* **2007**, *126*, 224305.

Table 1. Number of states available at various energies above the ground separated atom limit.[a]

| | Energy above the ground separated atom limit | | | | |
|---|---|---|---|---|---|
| Molecule | 100 $cm^{-1}$ | 500 $cm^{-1}$ | 1000 $cm^{-1}$ | 2000 $cm^{-1}$ | 5000 $cm^{-1}$ |
| OH | 10 | 18 | 18 | 18 | 18 |
| YC | 36 | 36 | 90 | 90 | 90 |
| TaSi | 16 | 36 | 36 | 36 | 162 |
| TiSe | 25 | 105 | 105 | 120 | 189 |
| WC | 9 | 9 | 9 | 36 | 207 |
| AlNi | 18 | 96 | 126 | 186 | 246 |
| VS | 20 | 102 | 242 | 252 | 522 |
| TiCo | 50 | 210 | 306 | 552 | 1038 |
| $V_2$ | 16 | 260 | 684 | 784 | 3364 |

[a] The entries in the table represent the total number of electronic states in the molecule in question that arise from separated atom limits lying within the specified energy above ground state atoms.

Table 2. Predissociation-based BDE measurements for metal diatomics and clusters. [a]

| Molecule | BDE (eV) | Reference | Molecule | BDE (eV) | Reference |
|---|---|---|---|---|---|
| AlV | 1.489(10) | 37 | VNi | 2.100(2) | 26 |
| AlCr | 2.278(2)[b] | 37 | NbCr | 3.0263(6) | 38 |
| AlCo | 1.844(2) | 37 | NbCo | 2.729(1) | 39 |
| AlNi | 2.459(1)[b] | 40 | NbNi | 2.780(1) | 39 |
| YCo | 2.591(1) | 39 | CrW | 2.867(1) | 41 |
| YNi | 2.904(1) | 39 | $Rh_2$ | 2.4059(5) | 39 |
| TiV | 2.068(1) | 26 | $Ni_2$ | 2.067(2)[b] | 42, 43 |
| TiCo | 2.401(1) | 26 | NiPt | 2.798(3) | 44 |
| TiZr | 2.183(1) | 45 | $Pt_2$ | 3.141(3)[b] | 46 |
| TiNb | 3.092(1) | 45 | $Ti_2^+$ | 2.435(2) | 27 |
| $Zr_2$ | 3.052(1) | 39 | $TiO^+$-Mn | 1.763(1) | 47 |
| ZrV | 2.663(3) | 45 | $V_2^+$ | 3.140(2) | 27 |
| ZrCo | 3.137(1) | 39 | $V_2^+$-V | 2.585(1)[b] | 47 |
| ZrNi | 2.861(1) | 39 | $Co_2^+$ | 2.765(1) | 27 |
| $V_2$ | 2.753(1) | 26 | $Co_2^+$-Co | 2.086(2) | 27 |

[a] This compilation only includes values measured in the Morse group.

[b] The originally published BDEs for AlCr, AlNi, $Ni_2$, $Pt_2$, and $V_2^+$-V were based on assumptions concerning whether they dissociate to the ground separation atom or not. Based on our more recent experience, all of the values listed in this table have been revised under the assumption that the molecules dissociate as soon as the ground state separated fragment limit is exceeded. Thus the values reported here differ from those published in the associated references for these particular species.

Table 3. Predissociation-based BDE measurements reported by other groups.

| Molecule | BDE (eV) | Reference | Molecule | BDE (eV) | Reference |
|---|---|---|---|---|---|
| VNb | 3.789(1) | 28 | $Co^+$-Fe | 2.69(22) | 48 |
| $Mo_2$ | 4.476(10) | 30 | $Co^+$-$CH_3$ | 2.47(30) | 49 |
| $Sc^+$-Fe | 2.08(22) | 48 | $Co^+$-$CH_2$ | 3.64(22) | 50 |
| $Ti^+$-Fe | 2.60(26) | 48 | $Co^+$-CH | 4.34(30) | 50 |
| $V^+$-Fe | 3.25(22) | 51 | $Co^+$-C | 3.90(60) | 50 |
| $V^+$-$C_6H_6$ | 2.69(22) | 49 | $Co^+$-$C_6H_6$ | 2.95(22) | 49 |
| $C_6H_6V^+$-$C_6H_6$ | 2.47(22) | 49 | $Co^+$-OH | 3.08(13) | 52 |
| $Cr^+$-Fe | 2.17(30) | 48 | $Co^+$-S | 2.69(22) | 49 |
| $Fe^+$-Fe | 2.69(22) | 48 | $Ni^+$-Ni | 2.32(2) | 31 |
| $Fe^+$-$CH_3$ | 2.82(22) | 49 | $Ni^+$-Fe | 2.78(22) | 48 |
| $Fe^+$-$CH_2$ | 3.56(22) | 50 | $Ni^+$-S | 2.60(22) | 49 |
| $Fe^+$-CH | 4.38(30) | 50 | $Ni^+$-$2C_2H_4$ | 3.47(22) | 49 |
| $Fe^+$-C | 4.08(30) | 50 | $Cu^+$-Fe | 2.30(30) | 48 |
| $Fe^+$-$C_6H_6$ | 2.39(22) | 49 | $Zr^+$-Zr | 4.18(1) | 32 |
| $Fe^+$-butadiene | 2.08(22) | 49 | $Nb^+$-Nb | 5.94(1) | 32 |
| $Fe^+$-O | 2.95(22) | 49 | $Nb_3^+$-Nb | 5.994(4) | 32 |
| $Fe^+$-S | 2.82(22) | 49 | $Nb^+$-Fe | 2.95(22) | 48 |
| $Fe^+$-OH | 3.17(13) | 52 | $Ta^+$-Fe | 3.12(22) | 48 |

Table 4. Predissociation-based BDE measurements for MX molecules (eV).[a]

| Sc | Ti | V | Cr | Mn | Fe | Co | Ni |
|---|---|---|---|---|---|---|---|
| C 3.042(10)[b] | C 3.857(4)[c] | C 4.109(3)[f] | C | C | C 3.961(19)[g] | C 3.899(13)[b] | C 4.167(3)[g] |
| N | N 5.015(12)[b] | N 4.997(2)[f] | N | N | N | N | N |
| Si 2.015(3)[b] | Si 2.201(3)[d] | Si 2.234(3)[d] | Si | Si | Si 2.402(3)[h] | Si 2.862(3)[h] | Si 3.324(3)[h] |
| S 4.852(10)[b] | S 4.690(4)[b] | S 4.535(3)[f] | S | S | S 3.240(3)[g] | S 3.467(5)[b] | S 3.651(3)[g] |
| Cl | Cl | Cl | Cl | Cl | Cl | Cl | Cl |
| Se | Se 3.998(6)[e] | Se 3.884(3)[e] | Se | Se | Se 2.739(6)[g] | Se | Se 3.218(3)[g] |
| **Y** | **Zr** | **Nb** | **Mo** | **Tc** | **Ru** | **Rh** | **Pd** |
| C 3.420(3)[b] | C 4.892(10)[c] | C 5.620(4)[c] | C | C | C | C | C |
| N | N | N | N | N | N | N | N |
| Si 2.450(2)[b] | Si 2.950(3)[d] | Si 3.080(3)[d] | Si | Si | Si 4.132(3)[h] | Si 4.169(3)[h] | Si |
| S 5.391(3)[b] | S 5.62(4)[b] | S 5.572(3)[b] | S | S | S 4.071(8)[b] | S 3.611(3)[b] | S |
| Cl | Cl | Cl | Cl | Cl | Cl | Cl | Cl |
| Se | Se 4.902(3)[e] | Se 4.834(3)[e] | Se | Se | Se | Se | Se |
| **La** | **Hf** | **Ta** | **W** | **Re** | **Os** | **Ir** | **Pt** |
| C 4.718(4)[b] | C 4.426(3)[c] | C 4.975(3)[c] | C 5.289(8)[i] | C | C | C | C |
| N | N | N | N | N | N | N | N |
| Si 2.891(5)[b] | Si 2.871(3)[d] | Si 2.999(3)[d] | Si 3.103(3)[i] | Si | Si 4.516(3)[h] | Si 4.952(3)[h] | Si 5.325(9)[h] |
| S | S 5.81(3)[b] | S 5.542(3)[b] | S 4.935(3)[i] | S | S 4.277(3)[b] | S | S |
| Cl | Cl | Cl | Cl 3.818(6)[i] | Cl | Cl | Cl | Cl |
| Se | Se 5.154(4)[e] | Se 4.705(3)[e] | Se 4.333(6)[i] | Se | Se | Se | Se |

[a] This compilation only includes values measured in the Morse group.

[b] Not yet published. Final published value may differ slightly from this report.

[c] Reference 36.

[d] Reference 35.

[e] Reference 34.

[f] Reference 33.

[g] Reference 53.

[h] Reference 54.

[i] Reference 55.

Table 5. Thermochemical Cycle Verification.[a]

| Molecule | IE(MX) | IE(M) | $D_0$(MX) | $D_0(M^+$-X) | Thermochemical Defect (Δ) |
|---|---|---|---|---|---|
| TiC | 6.5960(1)[b] | 6.82812[c] | 3.857(4)[d] | 4.05(24)[e] | 0.04 ± 0.24 |
| VC | 7.1358(10)[f] | 6.746187[c] | 4.109(3)[g] | 3.82(21)[h]<br>3.95(4)[i]<br>3.87(14)[e] | -0.10 ± 0.21<br>-0.23 ± 0.04<br>-0.15 ± 0.14 |
| VN | 7.05588(10)[j] | 6.746187[c] | 4.997(2)[g] | 4.65(6)[k] | 0.04 ± 0.06 |
| NbC | 6.9889(1)[l] | 6.75885[c] | 5.620(4)[d] | 5.28(15)[m] | 0.11 ± 0.15 |
| CoC | 7.73467(7)[n] | 7.88101[c] | 3.899(13)[o] | 3.60(30)[p] | 0.45 ± 0.30 |

[a] All quantities are listed in eV. The thermochemical defect, defined as $\Delta = D_0(MX) + IE(M) - IE(MX) - D_0(M^+-X)$, must be exactly zero by definition. When it deviates significantly, at least one of the component quantities must be in error.

[b] Reference 18.

[c] Reference 25.

[d] Reference 36.

[e] Reference 12.

[f] Reference 20.

[g] Reference 33.

[h] Reference 9.

[i] Reference 10.

[j] Reference 17.

[k] Reference 11.

[l] Reference 19.

[m] Reference 14.

[n] Reference 16.

[o] Not yet published.

[p] Reference 13.

Figure Captions:

Figure 1. Qualitative potential energy curves for OH. Adapted with permission from ref. 22. Copyright 1981 IOP Publishing.

Figure 2. Potential energy curves of YC and $YC^+$. Adapted with permission from ref. 56. Copyright 2007 American Institute of Physics.

Figure 3. Integrated density of electronic states in transition metal molecules (and OH) as a function of energy above the ground separated atom limit. All but OH show a sharp predissociation threshold that is interpreted as the bond dissociation energy.

Figure 4. The resonant two-photon ionization process. The molecule is excited to an excited electronic state by absorption of photon $h\nu_1$, and is subsequently ionized by absorption of photon $h\nu_2$. Neither photon has sufficient energy to ionize the molecule in a one-photon process.

Figure 5. Predissociation threshold for diatomic TiCo. Reproduced from ref. 26.

Figure 6. Thermochemical cycle relating the bond energies of $V_2$ and $V_2^+$.

Figure 7. Predissociation threshold in diatomic VS. Reproduced with permission from ref. 33. Copyright 2016 American Institute of Physics. The vanadium atomic spectrum was used for calibration.

Figure 8. Predissociation threshold in diatomic TaSi. Reproduced with permission from ref. 35. Copyright 2017 American Institute of Physics.

Figure 9. Predissociation threshold in diatomic TiSe. Reproduced with permission from ref. 34. Copyright 2016 American Institute of Physics.

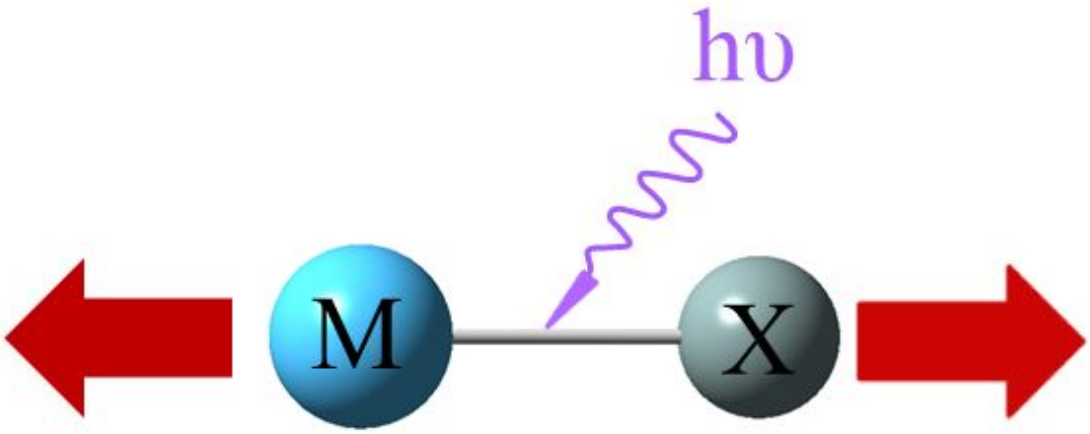
hυ
M
X

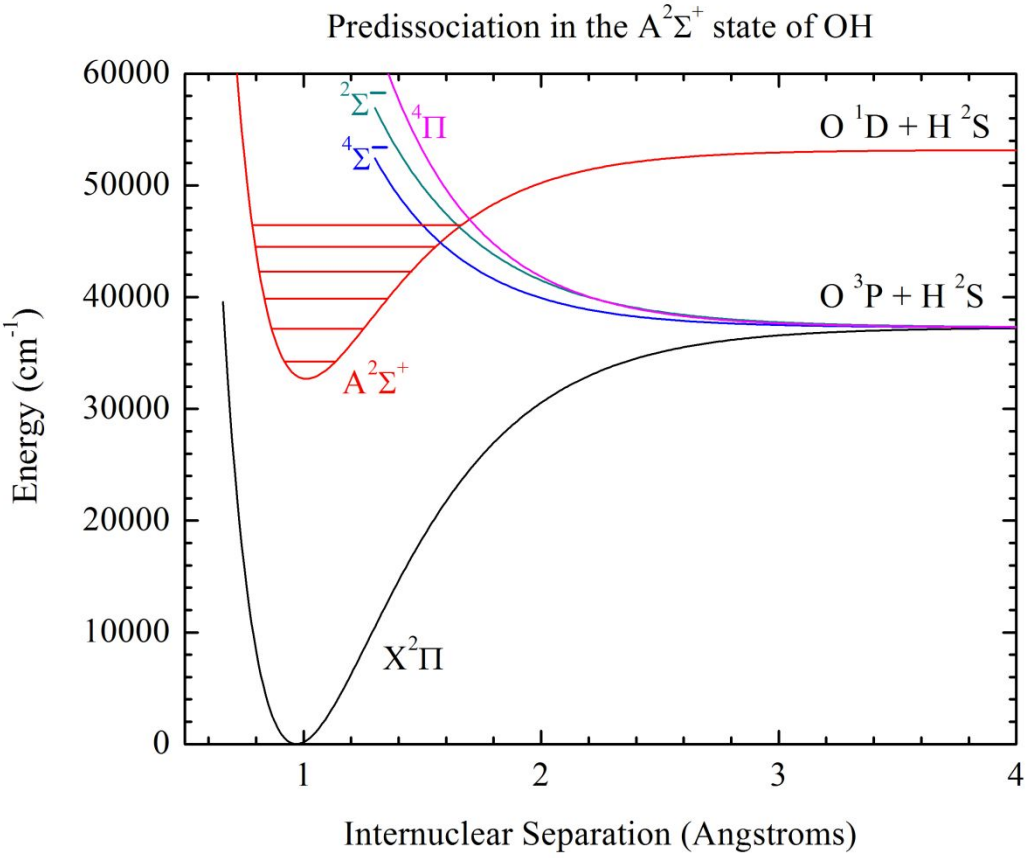


Figure 1. Qualitative potential energy curves for OH. Adapted with permission from ref. 22. Copyright 1981 IOP Publishing.

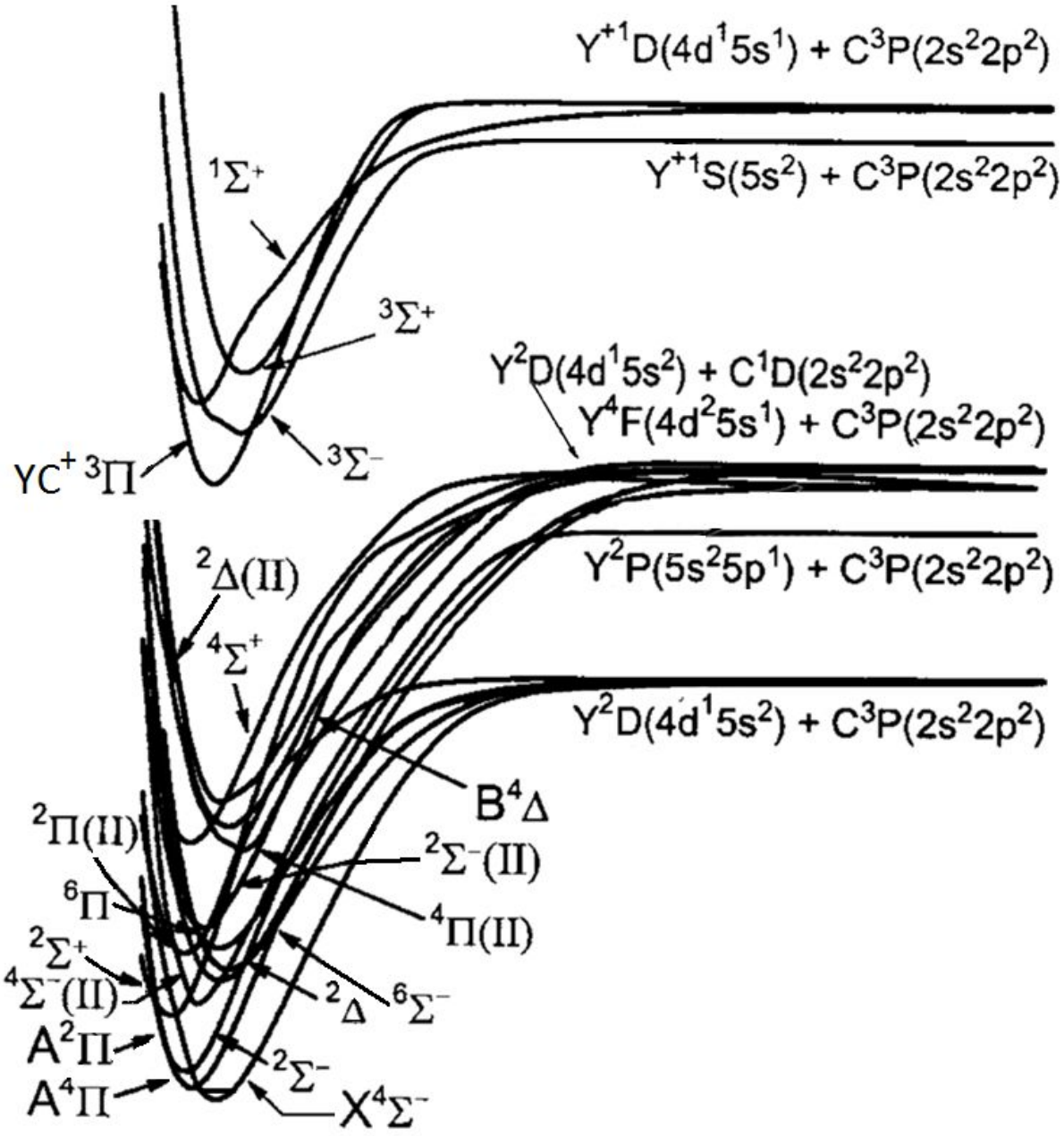


Figure 2. Potential energy curves of YC and $YC^+$. Adapted with permission from ref. 56. Copyright 2007 American Institute of Physics.

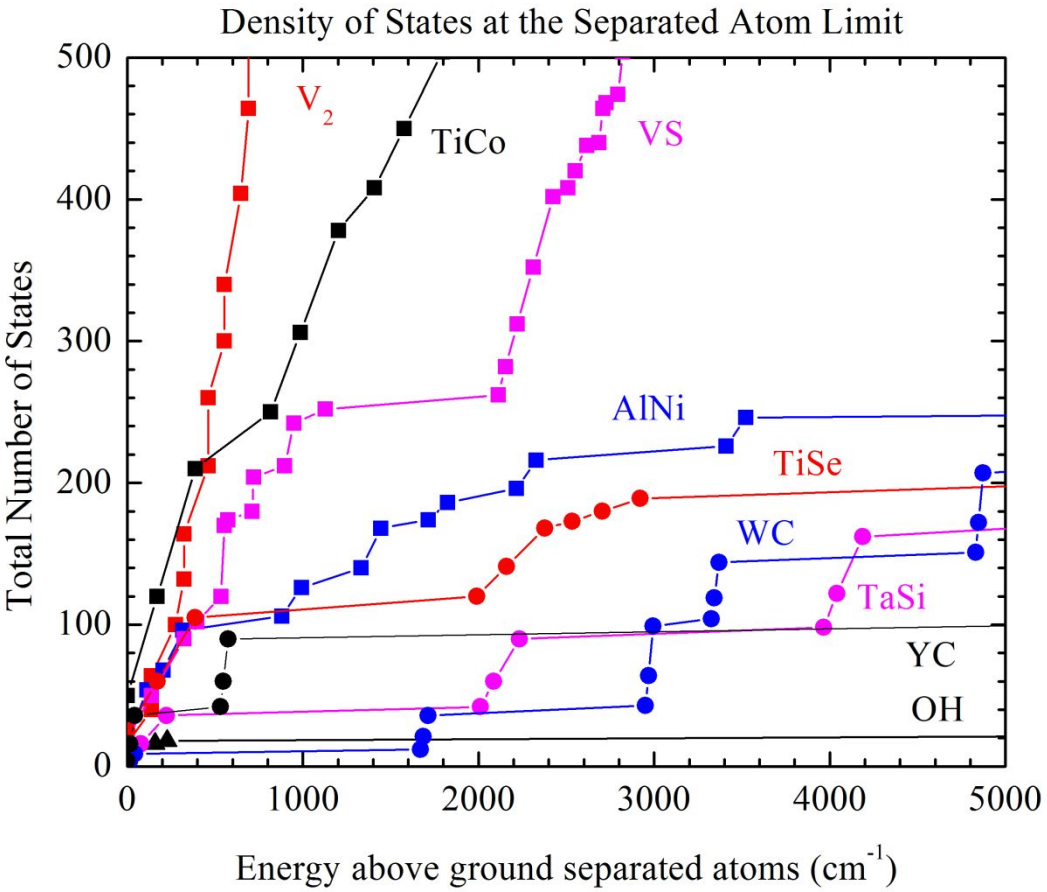


Figure 3. Integrated density of electronic states in transition metal molecules (and OH) as a function of energy above the ground separated atom limit. All but OH show a sharp predissociation threshold that is interpreted as the bond dissociation energy.

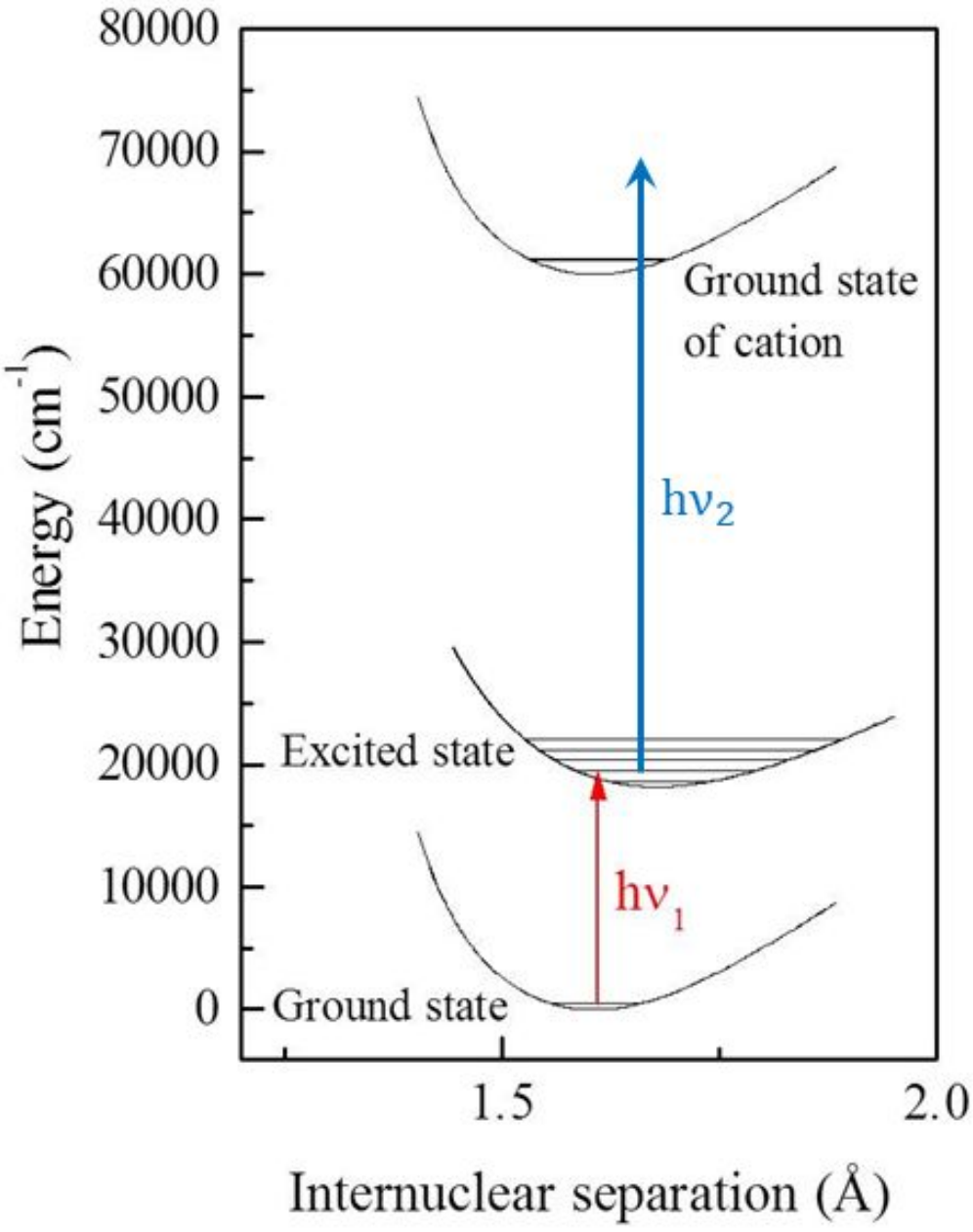


Figure 4. The resonant two-photon ionization process. The molecule is excited to an excited electronic state by absorption of photon $h\nu_1$, and is subsequently ionized by absorption of photon $h\nu_2$. Neither photon has sufficient energy to ionize the molecule in a one-photon process.

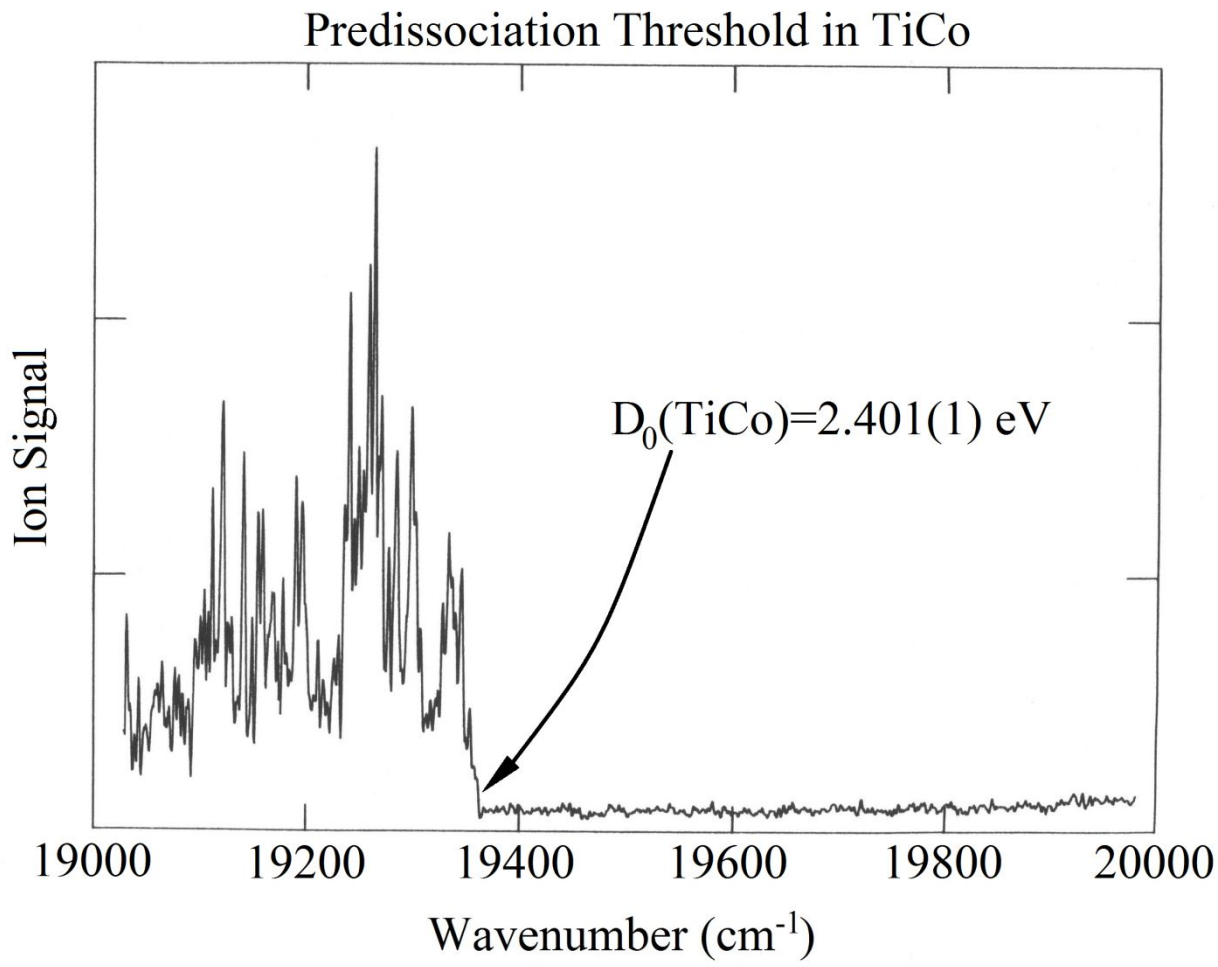


Figure 5. Predissociation threshold for diatomic TiCo. Reproduced with permission from ref. 26. Copyright 1992 American Chemical Society.

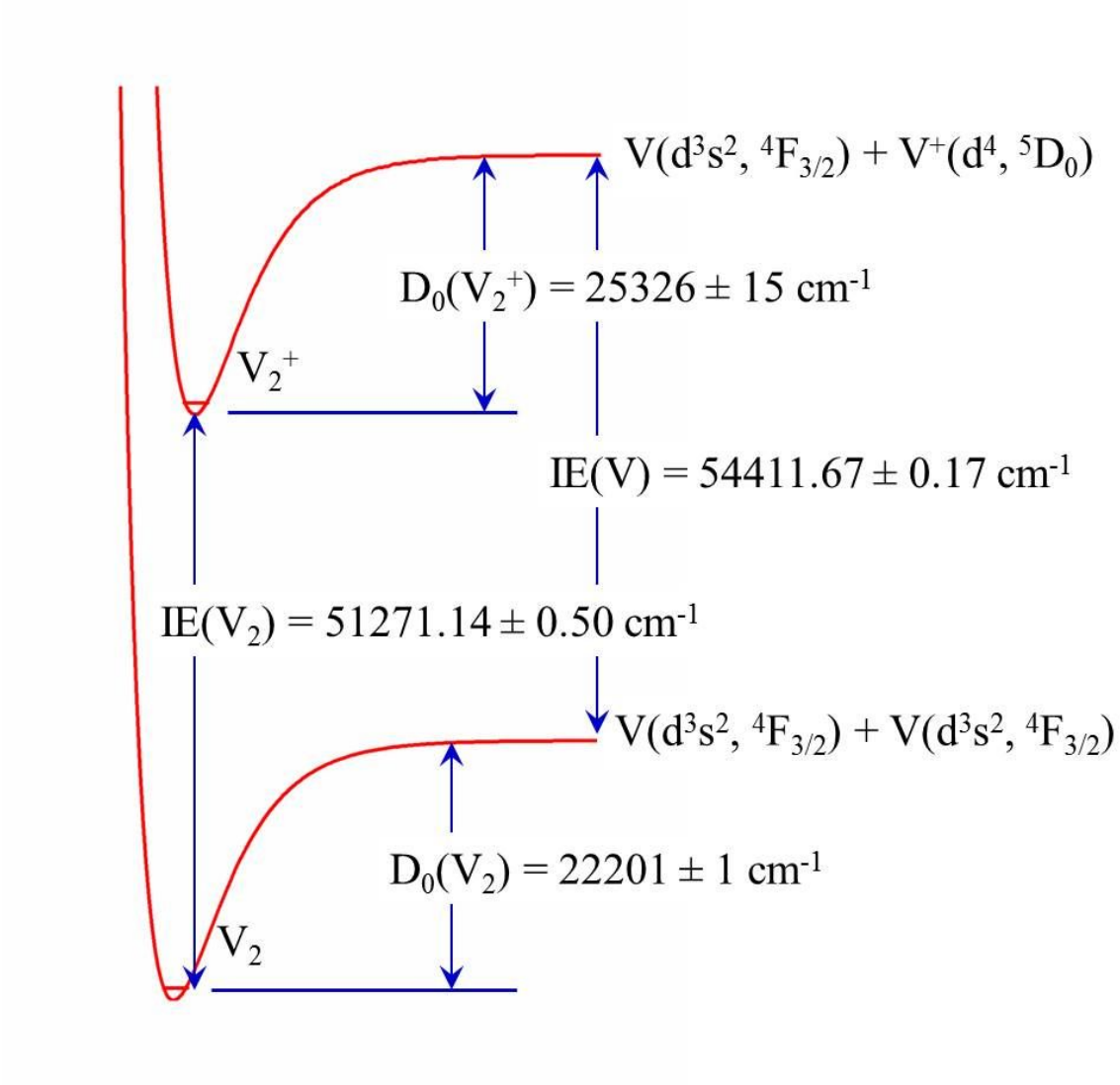


Figure 6. Thermochemical cycle relating the bond energies of $V_2$ and $V_2^+$.

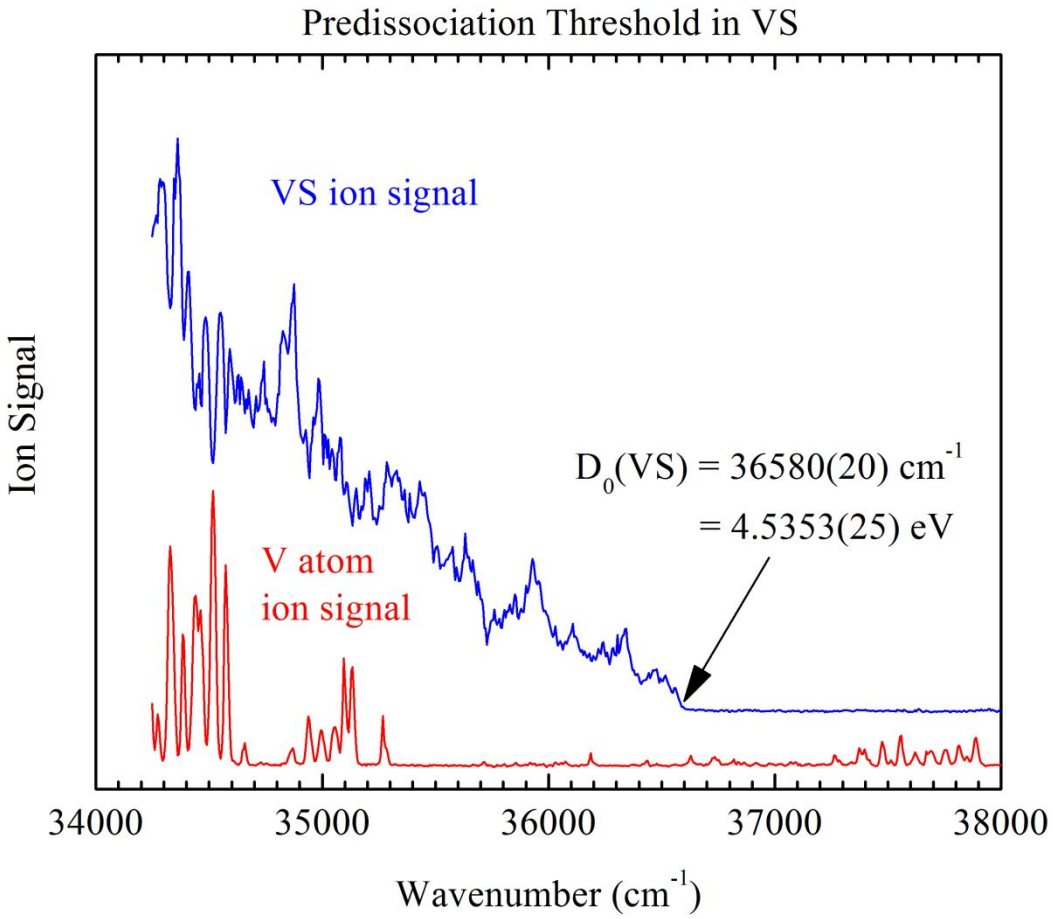


Figure 7. Predissociation threshold in diatomic VS. Reproduced with permission from ref. 33. Copyright 2016 American Institute of Physics. The vanadium atomic spectrum was used for calibration.

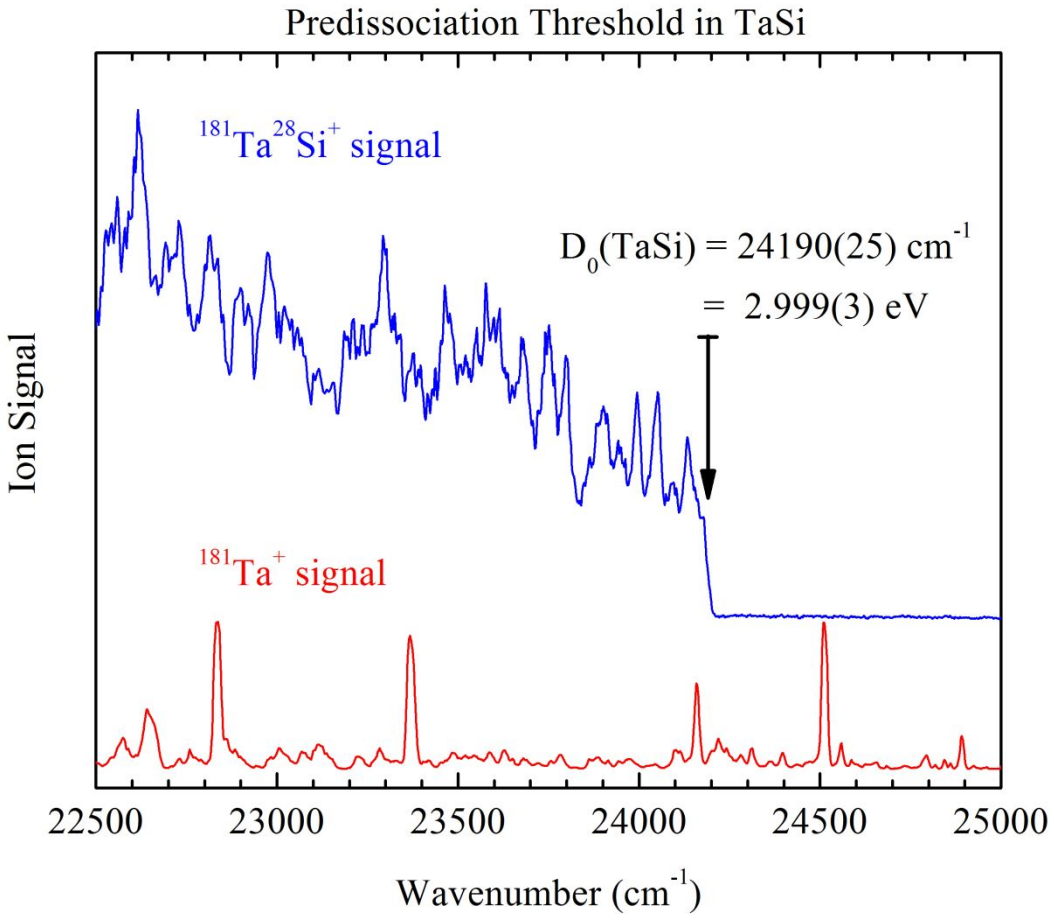


Figure 8. Predissociation threshold in diatomic TaSi. Reproduced with permission from ref. 35. Copyright 2017 American Institute of Physics.

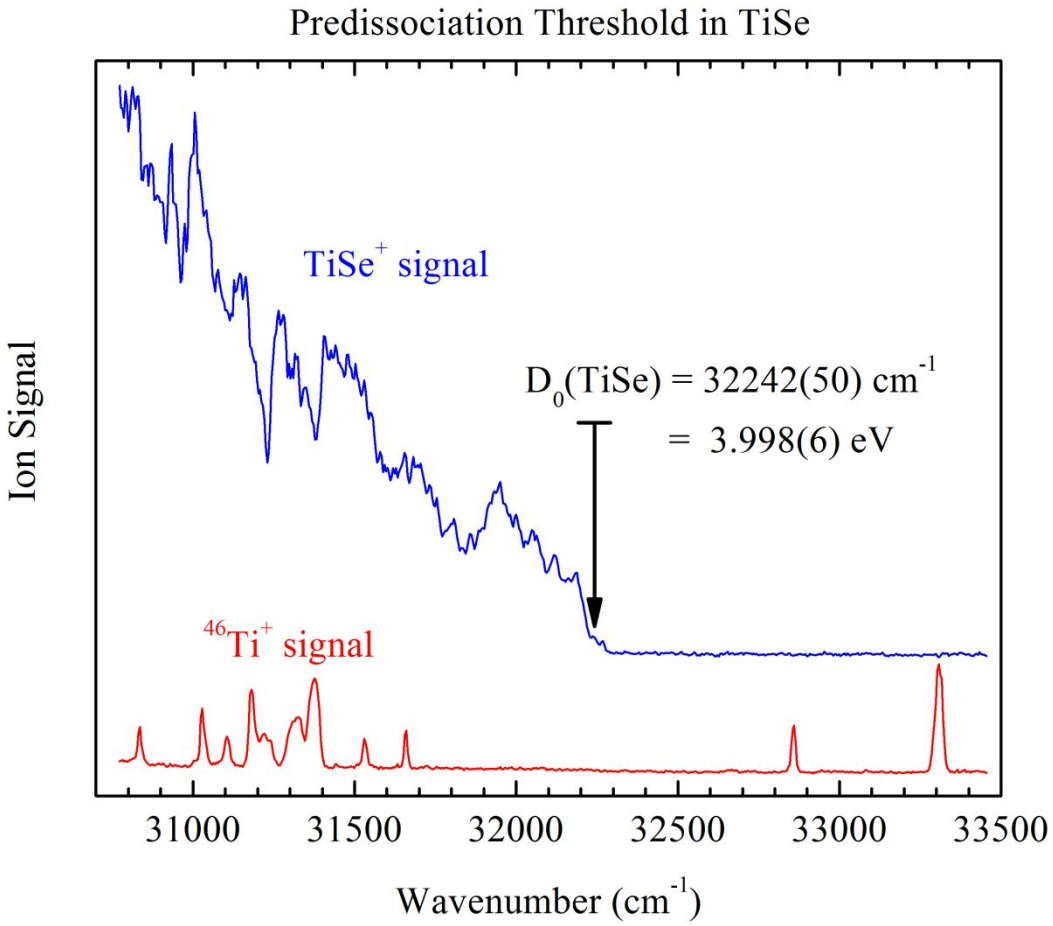


Figure 9. Predissociation threshold in diatomic TiSe. Reproduced with permission from ref. 34. Copyright 2016 American Institute of Physics.

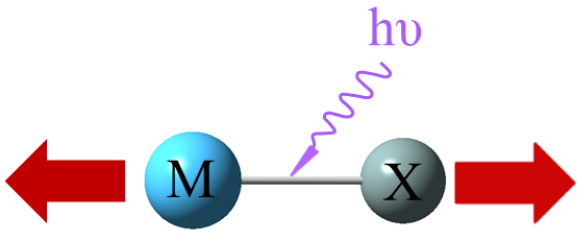


254x190mm (96 x 96 DPI)

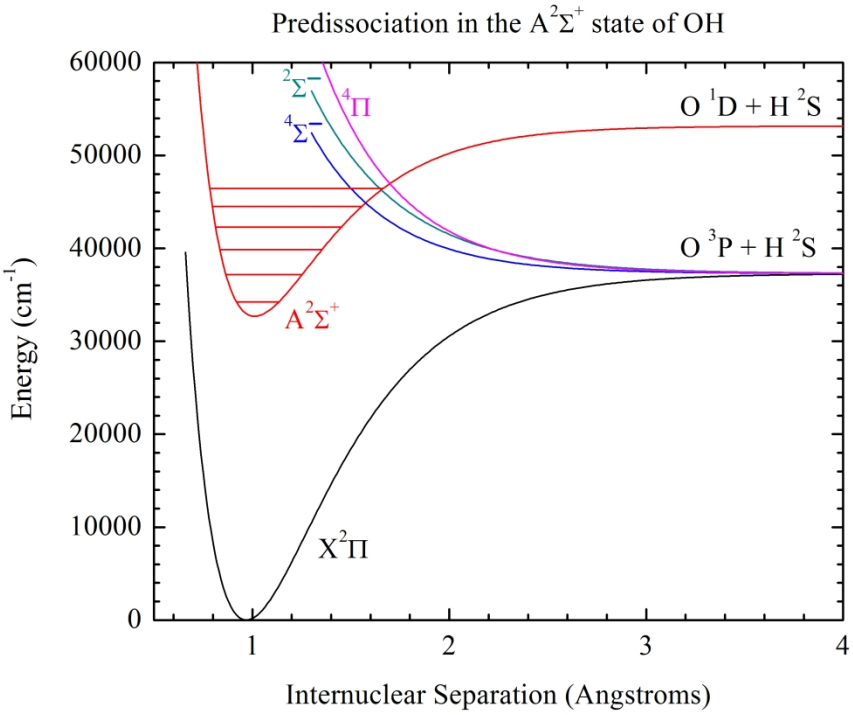


Figure 1. Qualitative potential energy curves for OH. Adapted with permission from ref. 22. Copyright 1981 IOP Publishing.

267x217mm (300 x 300 DPI)

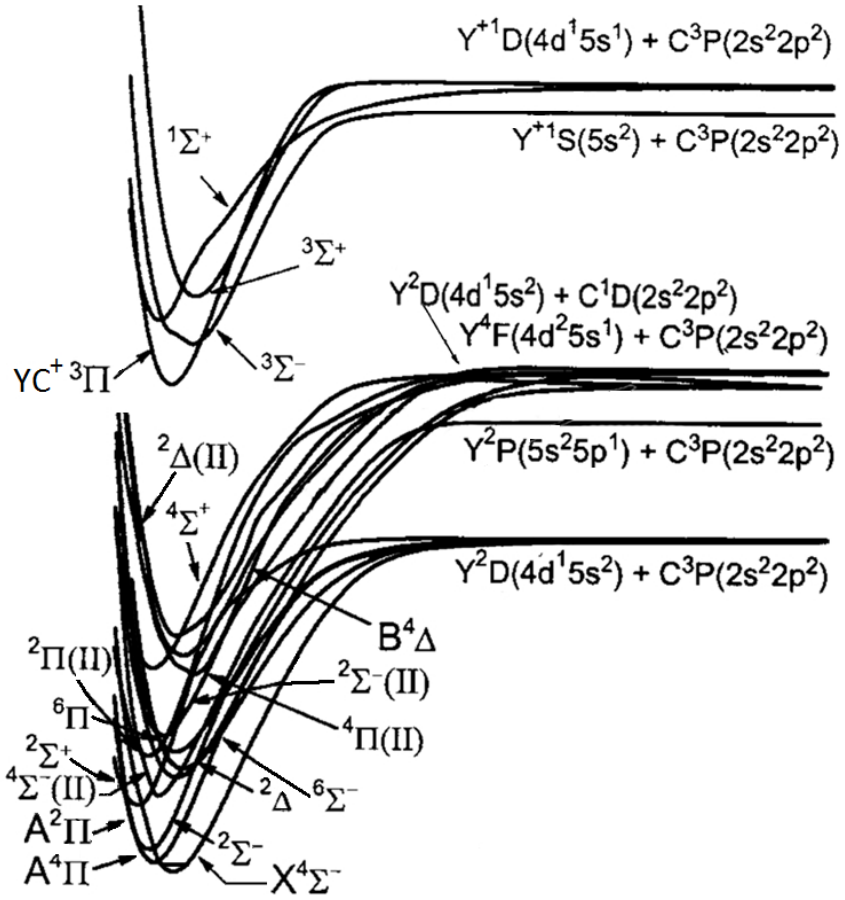


Figure 2. Potential energy curves of YC and YC+. Adapted with permission from ref. 56. Copyright 2007 American Institute of Physics.

196x277mm (96 x 96 DPI)

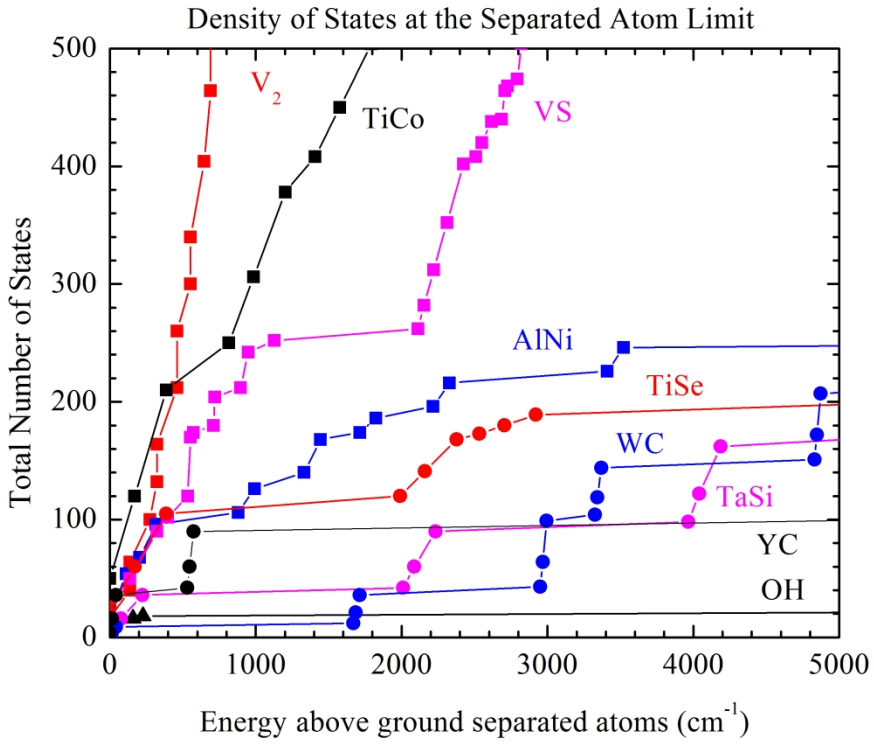


Figure 3. Integrated density of electronic states in transition metal molecules (and OH) as a function of energy above the ground separated atom limit. All but OH show a sharp predissociation threshold that is interpreted as the bond dissociation energy.

253x214mm (300 x 300 DPI)

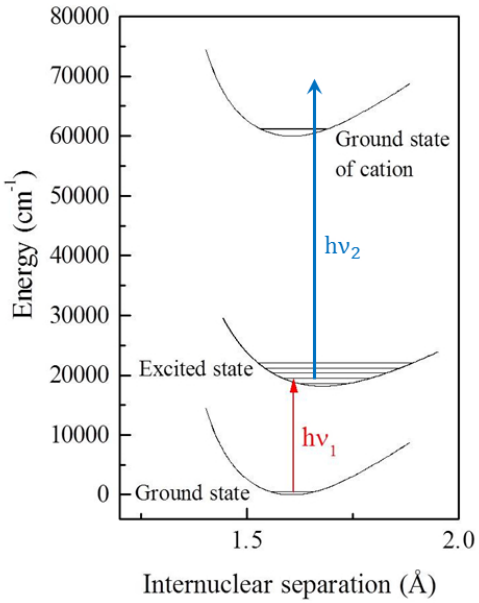


Figure 4. The resonant two-photon ionization process. The molecule is excited to an excited electronic state by absorption of photon $h\nu_1$, and is subsequently ionized by absorption of photon $h\nu_2$. Neither photon has sufficient energy to ionize the molecule in a one-photon process.

254x190mm (96 x 96 DPI)

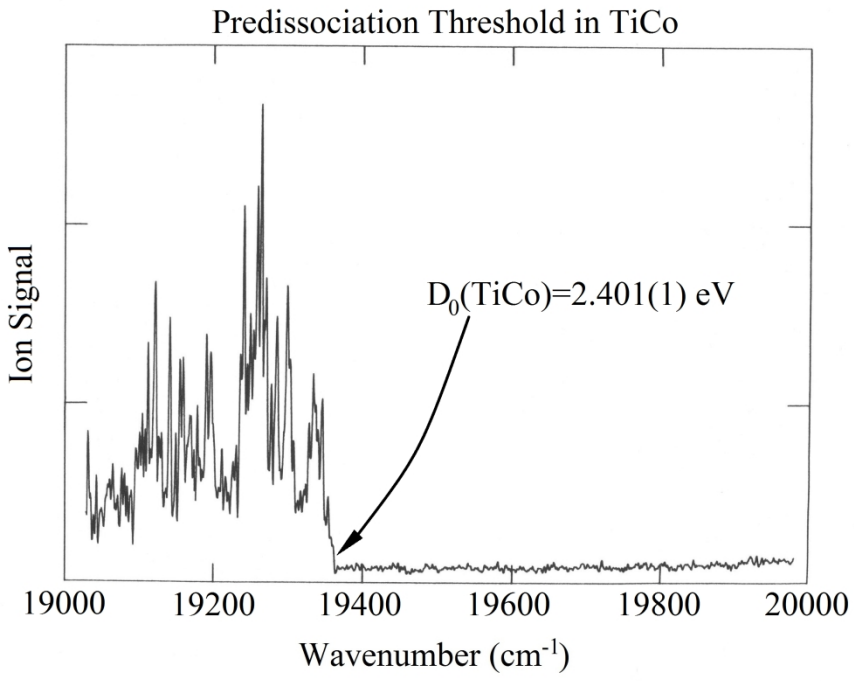


Figure 5. Predissociation threshold for diatomic TiCo. Reproduced from ref. 26.

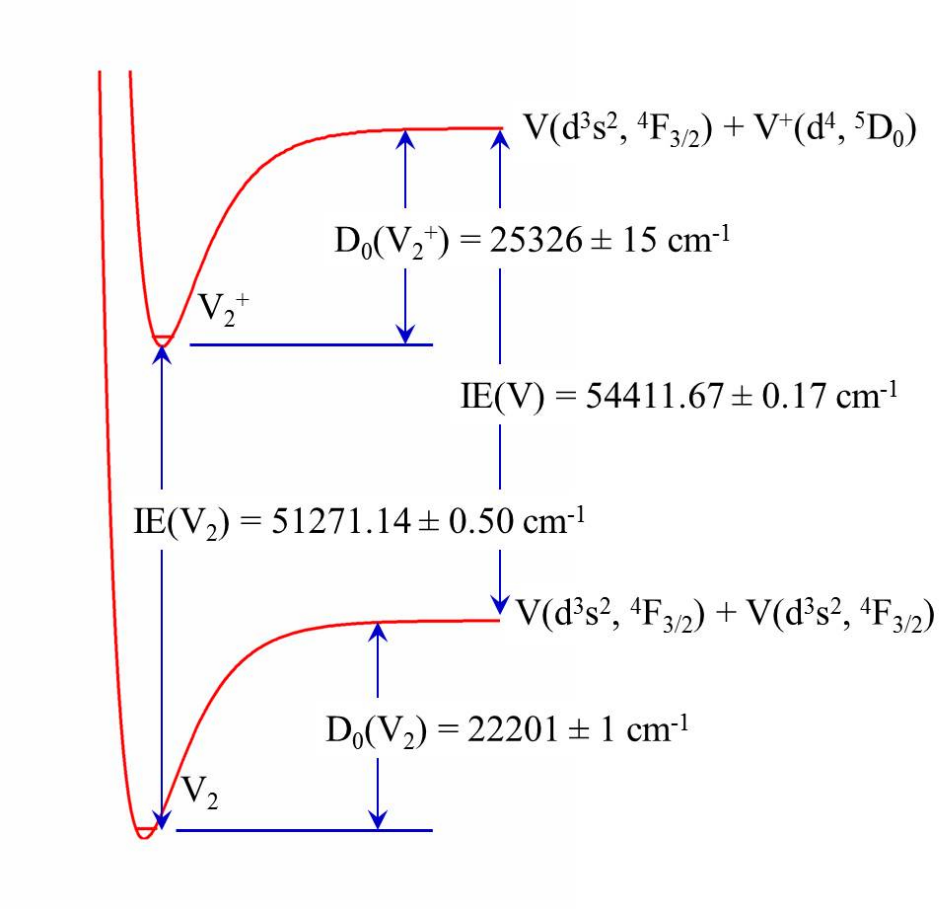


Figure 6. Thermochemical cycle relating the bond energies of $V_2$ and $V_2^+$.

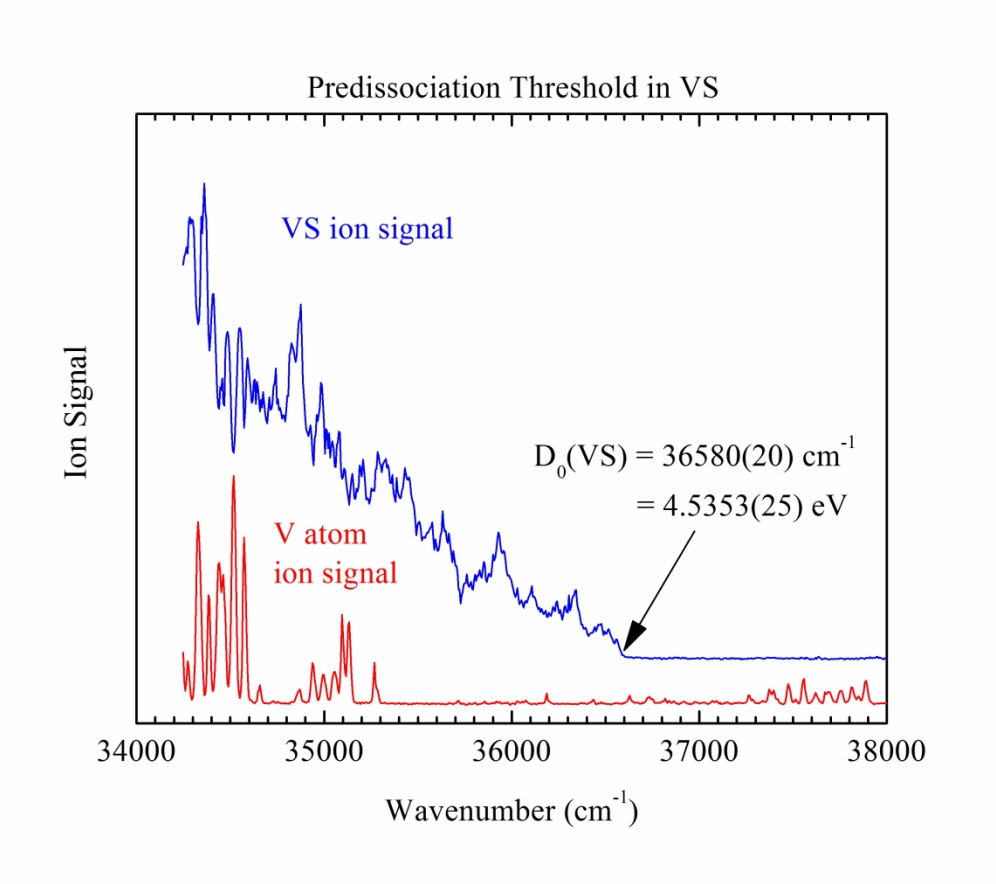


Figure 7. Predissociation threshold in diatomic VS. Reproduced with permission from ref. 33. Copyright 2016 American Institute of Physics. The vanadium atomic spectrum was used for calibration.

244x216mm (300 x 300 DPI)

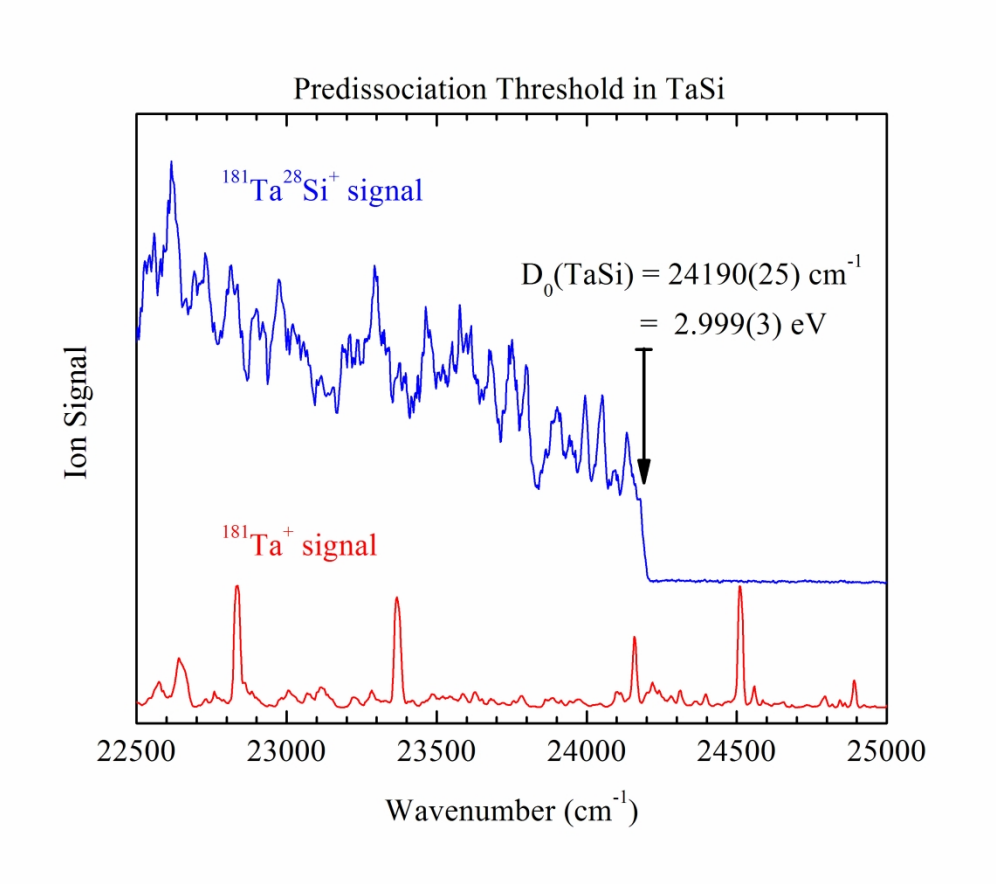


Figure 8. Predissociation threshold in diatomic TaSi. Reproduced with permission from ref. 35. Copyright 2017 American Institute of Physics.

244x216mm (300 x 300 DPI)

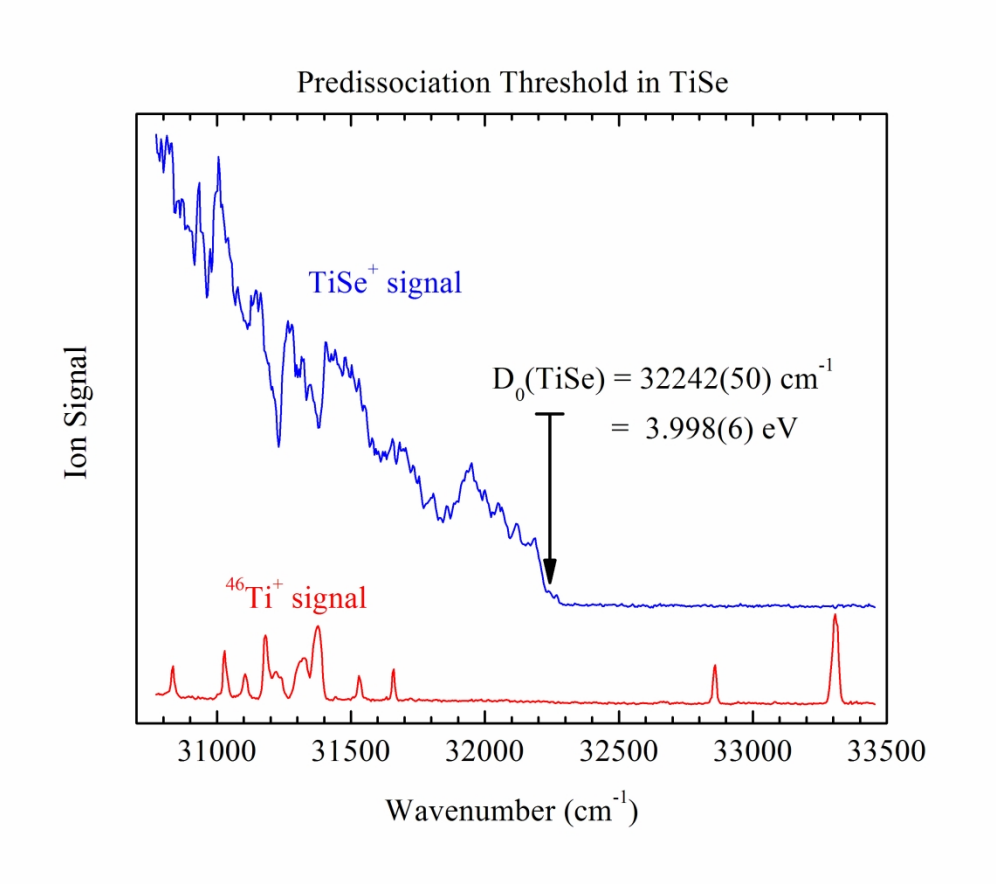


Figure 9. Predissociation threshold in diatomic TiSe. Reproduced with permission from ref. 34. Copyright 2016 American Institute of Physics.

244x216mm (300 x 300 DPI)